Optical Metacages

Ali Mirzaei,[*] Andrey E. Miroshnichenko, Ilya V. Shadrivov, and Yuri S. Kivshar

Nonlinear Physics Centre, Research School of Physics and Engineering, Australian National University, ACT 2601, Australia

We suggest a novel strategy for spectrally selective optical shielding of arbitrary shaped volumes by arranging specifically designed two- or three-layer nanowires around an area that needs to be protected. We show that such nanowire shields preserve their functionality for almost arbitrary geometry, and we term such structures *optical metacages*. We analyze several designs of such optical metacages made from either metallic or dielectric materials with experimentally measured parameters. We employ a semianalytical approach and also verify our results by numerical simulations. We further study optical properties of the introduced metacages in both near- and far-field regions, as well as analyze their frequency selectivity and the vanishing backscattering regime.

Nanophotonics is finding its way toward modern applications. In communication and signal processing, the electronic signal transmission between the integrated circuit elements is expected to be replaced by optical signals [1,2]. This would require scaling down laser sources [3] and light detectors [4], for efficient on-chip integration. This is why creating an optical isolation between different components is an extremely important task for eliminating unwanted interferences.

In medicine, new techniques for drug delivery based on optical control of shielded nanostructures attract a growing interest. It became possible to achieve near-complete drug release from hollow gold nanoshells by illuminating them with laser pulses [5,6] or by microwave radiation of magnetic core-shell nanocarriers [7]. Cubic gold nanocages can be used for controlled drug release, based on photothermal effects and absorption of near-infrared light [8–10], while the organometallic cages can hide photosensitizers to facilitate their delivery to cancer cells [11]. The vesicles covered by gold nanoparticles are unusually stable to high temperatures, chromatographic purification, and high salt concentrations—the conditions which are too harsh for ordinary self-assembled vesicles to survive [12].

The shielding of objects from the optical radiation should also benefit many other research areas. For example, such functionality was predicted with metamaterials [13,14], graphene sheets [15], and epsilon-near-zero or epsilon-very-large materials [16]. However, the proposed shielding structures have various limitations, i.e., they can cover either only small subwavelength objects, or only specific geometries, they may require inhomogeneous and/or magnetic materials, and some of the designs do not work in the optical frequency range.

Various thin absorbing structures have been studied for different frequency ranges, ranging from visible [17,18] and infrared [19–21] to THz [22] and GHz [23]. Perfect symmetric absorbing structures [24,25], with zero reflection

and transmission from either side, have recently attracted considerable attention in THz [26,27] and GHz [28] frequency ranges.

In this Letter, we introduce a novel approach for designing ultrathin optical shielding nanostructures ("metacages"), with symmetric functionality across the visible and infrared range, and in both nano- and micrometer scales. We study metashielding structures made of long nanowires composed of realistic materials, enclosing relatively large volumes, which can operate with a considerable space between the nanowires. In our work, we do not aim to design perfect absorbers (that can also create fully shielded structures), but instead we design metacages with large gaps between their constituent elements. This condition can be useful for integrated optics since it allows us to make shielded spaces of arbitrary shapes. In biological applications, such metacages can be employed to protect live microorganisms and cells from electromagnetic radiation, while keeping them alive inside the shielded volume in lab-on-a-chip structures by enabling the access of liquids and gases from outside. We show that these nanostructures can operate independently of their shape, being designed effectively in a wide spectral range.

Using well-spaced nanowires as building blocks of metacages is not only a proper choice to provide a considerable physical space to connect the sides, but also offers flexible design capabilities. Two examples of the analyzed structures are demonstrated in Figs. 1(a) and 1(b) with shielding achieved for a structure with the shape of Australia. Such shields work for any angle of incidence of light, and for any position of the source inside the structure, as demonstrated in the Supplemental Material [29]. In what follows, we consider long nanowires, and analyze the metacages as two-dimensional structures.

We use the multipole expansion and multiple scattering methods to study analytically the optical properties of nanowire structures. We assume that all nanowires are
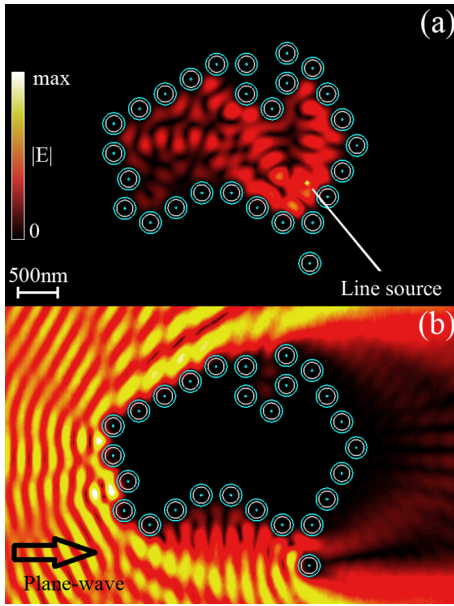
FIG. 1 (color online). Demonstration of metacage functionalities for an arbitrary shape (here is an outline of Australia) made of multilayer nanowires. (a) Radiation of a point source placed inside the metacage is contained within the structure. (b) A volume inside the metacage is screened from an incident plane wave. Three-layer Si-Ag-Si nanowires are used to form the metacage. The amplitude of the electric field is plotted at $\lambda = 378$ nm, using the commercial software CST Microwave Studio. The design parameters are found by an analytical approach, and are summarized in Table I (see also [29]).

identical, and the gaps between the adjacent nanowires are equal. For TM polarization (the electric field parallel to nanowires' axes), the incident plane wave can be written as $\mathbf{E}^{\mathrm{inc}} = \hat{\mathbf{a}}_z E_0 \exp[-i\omega t + i2\pi\lambda^{-1} r \cos(\varphi)]$, where φ is the polar angle in cylindrical coordinates. Using the multipole expansion method [30,31], the total field in the layer l of an L-layered individual multilayer nanowire can be presented as

$$\mathbf{E}^l_{\mathrm{total}} = \hat{\mathbf{a}}_z E_0 \exp[-i\omega t]$$
$$\times \sum_{n=-\infty}^{+\infty} e^{in[\varphi+(\pi/2)]} [\tau^l_n J_n(\beta_l r) + \rho^l_n H^{(1)}_n(\beta_l r)], \quad (1)$$

where $\beta_l = (2\pi/\lambda)\sqrt{\epsilon_l(\lambda)}$, E_0 is the incident-plane-wave amplitude, J_n and $H^{(1)}_n$ are the nth order Bessel and Hankel functions of the first kind, respectively; n is the mode number, l is $L+1$ for the surrounding material (we consider air), $\epsilon_l(\lambda)$ is the dielectric constant of the lth layer at the wavelength λ, and r is the radius. Coefficients for partial waves in the lth layer, τ^l_n and ρ^l_n are found by satisfying the boundary conditions for the tangential components E_z and H_φ. Additionally, we put $\rho^1_n = 0$ to avoid singularity of Hankel functions in the center of the nanowires, and $\tau^{L+1}_n = 1$ for each mode to describe the

incident plane wave expansion through the cylindrical waves. For the TE polarization, an expression similar to Eq. (1) can be written for H^l_{total} and the expansion coefficients can be found by satisfying the boundary conditions for the tangential components of the fields, H_z and E_φ [32]. We also consider the small-size effect in plasmonic nanoparticles, which leads to corrections in the dielectric constants as compared to the bulk materials as a result of the collision frequency modification [33,34].

As the first step, we solve the boundary condition equations for an individual nanowire and find the expansion coefficients [30,31]. Solving boundary-value equations, we find τ^l_n and ρ^l_n. As the second step, we employ the multiple scattering problem solution, to consider the interaction between the nanowires [35–39]. The scattered field from one cylinder contributes to an incident wave on the other cylinders in addition to the incident plane wave. This leads to modified expansion coefficients ρ^{air}_n for every nanowire. As the third step, we calculate the fields inside the nanowires by modifying τ^l_n and ρ^l_n coefficients for all the layers of each nanowire by satisfying the boundary conditions.

We start with analyzing a single, three-layer nanowire made of gallium arsenide [40] and silver [41], as shown in Fig. 2(a). The choice of materials is discussed in the Supplemental Material [29] along with the material parameters used in the simulations. Figure 2(a) represents the cross section of a three-layer nanowire. The power flow is shown along with the calculated saddle point and the separatrices [42,43]. The separatrices indicate the boundary of two regions marked in Fig. 2(a): (i) a region in which energy flow streamlines pass through the nanowire, leading to the absorption of light, and (ii) a region where the energy flows around the structure without being absorbed.

Our main idea is to form metacages with large gaps between the elements, but still scattering and absorbing most of the light by making an array of nanowires, as demonstrated schematically in Fig. 2(b). Overlapping the separatrices of individual nanowires eliminates the energy flow that is not affected by the nanoparticles [region 2 of Fig. 2(a)]. Such an array of nanowires can block the electromagnetic waves propagating through the structure. In general, not all this energy is scattered or absorbed by the nanowires, and this causes some power leakage. This effect can be quantified, and a careful design of nanowire structures allows us to maximize the absorption and to decrease considerably the energy penetrating through the shield.

The joint separatrices and the formation of a shielding structure is demonstrated in Fig. 2(c). This figure shows the functionality of a *shielding metawall* in the middle of an array made of twelve nanowires separated by gaps which are larger than their radius. Once the separatrices are overlapped, by keeping the gap size below a certain threshold value, the shielding array operates independently
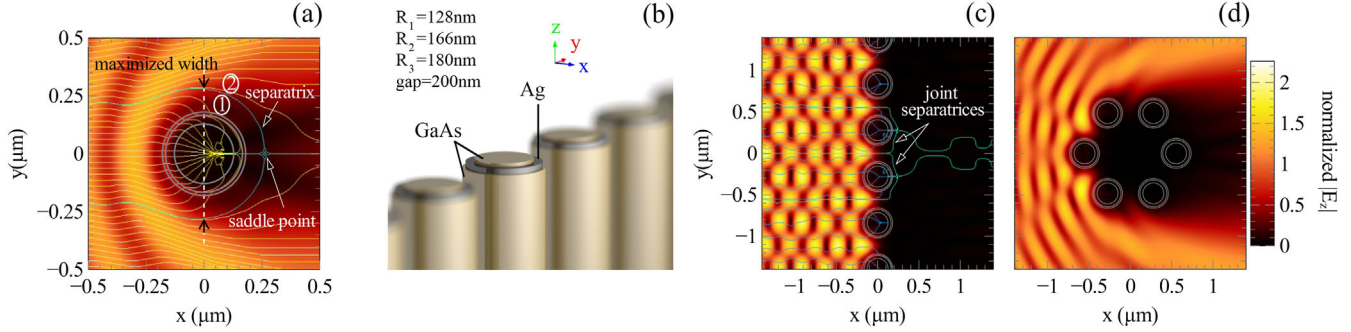
FIG. 2 (color online). Design of metacages. (a) Wave interaction with a single nanowire, color map shows the field profile, thin lines show the Poynting vectors. Separatrices of the energy flow divide the space into two parts, with energy flowing into the nanowire or going around it. (b) Schematics of the array of multilayer nanowires. (c) A one-dimensional chain of nanowires, which blocks the light propagation. (d) Enclosed volume shielded by nanowires, which can have an almost arbitrary shape (see, e.g., Fig. 1). Design parameters are summarized in Table I.

of its shape. As an example, Fig. 2(d) shows a closed array of similar nanowires with the similar gap as in Fig. 2(c). This is a simple form of a metacage which does not allow electric and magnetic fields to penetrate inside.

We note that the maximum spacing allowed between the nanowires is not directly proportional to the maximum spacing between separatrices of *individual* nanowires shown in Fig. 2(a) by a dashed line. This is caused by the interaction between nanowires that we account for in the multiple scattering method. In order to increase the spacing, we perform the numerical optimization and find that the optimal period of the array is less than the maximized width between the separatrices for an individual nanowire. Such an optimization can be done for any desired operation wavelength and for a given set of materials. Dependence of the metacage performance on the spacing between the nanowires is summarized in the Supplemental Material [29].

The separatrices of the energy flow responsible for the optimal separation of nanowires can be easily calculated by finding the saddle points. To do so, we use the fact that there is no energy flowing through these singular points. In cylindrical coordinates for TM polarized waves the Poynting vector characterizing the energy flow is $\mathbb{P}_{av} = \frac{1}{2}\text{Re}\{E \times H^*\}$, being expressed as

$$\mathbb{P}_{av} = \frac{1}{2}[-\hat{a}_r(E_z^R H_\varphi^R + E_z^I H_\varphi^I) + \hat{a}_\varphi(E_z^R H_r^R + E_z^I H_r^I)], \quad (2)$$

where the superscripts R and I indicate the real and imaginary parts, and the fields are functions of r and φ. Solving the equation $\mathbb{P}_{av} = 0$ gives us the locations of the saddle points. For the nanowire shown in Fig. 2(a) we find $x_{saddle} = 262.5$ nm. However, in the twelve-element array shown in Fig. 2(c), the saddle point shifts to $x_{saddle} = 237.2$ nm for two nanowires in the middle of the array, due to the multiple scattering and interaction between the nanowires. Once we obtain the saddle points, we choose points close to it (± 1 nm in the x and y directions in our

study) and calculate the energy flow using Eq. (2), to plot the separatrices, as shown in Fig. 2.

If we increase the gap between the nanowires so that the separatrices of the adjacent nanowires split, the electromagnetic energy will penetrate into the structure. On the other hand, by decreasing the gap, we suppress the field inside the metacage further and increase the bandwidth of its operation. With a small gap (5–20 nm) between the nanowires, it is possible to achieve wideband shielding, up to hundreds of nanometers, depending on the materials used. For example, by using GaAs nanowires a considerable shielding bandwidth is achievable from very short wavelengths ($\lambda < 300$ nm) up to around $\lambda = 450$ nm. With such a close spacing, the bandwidth follows the absorption of the material used in the nanowire construction and the spectrum of the imaginary part of the dielectric constant. Our study shows that shielding bandwidths up to $\lambda = 370$ nm and $\lambda = 600$ nm is possible by using Si and Ge nanowires, respectively.
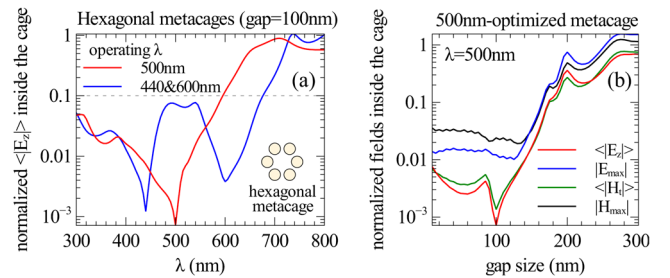
FIG. 3 (color online). (a) Two different hexagonal metacages designed for operation at three different wavelengths (TM polarization) by optimizing the radii of the layers. An average value of the field amplitude inside metacages remains under 0.1 of the incident wave amplitude across a considerable spectral range. Metacages are made of GaAs-Ag-GaAs multilayer nanowires with radii $R_{1-3} = 72, 165$, and 200 nm and $R_{1-3} = 60, 124$, and 187 nm for the red and blue curves, respectively. (b) Variation of the fields amplitude inside the metacage of (a) (red curve) vs the gap size.

TABLE I. The design parameters of various metacages made of multilayer nanowires with different materials. The average and maximum fields values indicate $|E|$ inside a hexagonal cage with external incident plane wave. The fields value as well as normalized scattering and absorption cross sections (NSCS & NACS) are calculated using the first 30 harmonics (see also Ref. [29]).

	Polarization	λ (nm)	R (nm)	Gap(nm)	Configuration	Average	Maximum	NSCS	NACS	Figures
1	TM	378	11,102,137	100	Si-Ag-Si	4.2×10^{-4}	4.5×10^{-3}	6.68	2.46	Fig. 1
2	TM	453	128,166,180	200	GaAs-Ag-GaAs	5.6×10^{-3}	5.5×10^{-2}	7.01	4.08	Fig. 2
3	TM	500	72,165,200	100	GaAs-Ag-GaAs	7.2×10^{-4}	1.2×10^{-2}	8.30	1.21	Fig. 3 (red)
4	TM	440	60,124,187	100	GaAs-Ag-GaAs	1.2×10^{-3}	2.3×10^{-3}	6.79	0.73	Fig. 3 (blue)
5	TM	449	138,148,158	100	GaAs-TiN-GaAs	1.0×10^{-2}	2.7×10^{-2}	5.58	3.06	Fig. 4

Despite the improvement of the shielding quality for the closer placed nanowire, this suppresses the physical connection between the inside and outside of the metacage. A compromise between the larger gap size and the field suppression can be achieved by designing metashields (see Fig. 3). We can ensure the uniformity of the electromagnetic field suppression inside the cage by keeping both the maximum and average field amplitude close to each other during the optimization process.

An interesting peculiarity of metacages made of multilayer nanowires is their capability to be designed for frequencies across a wide spectral range. Figure 3 demonstrates how modifying the size parameters of the GaAs-Ag-GaAs nanowires in a hexagonal metacage makes it possible to achieve shielding for the visible range. In this figure, two metacages are compared with the same gap size of 100 nm. The cage designed for the wavelength of 500 nm has stronger field suppression than the cage designed for 440 nm, but it has smaller relative spacing between the nanowires with respect to the nanowires' outer radius. The results show that it is also possible to design metacages for two different wavelengths simultaneously. Figure 3(a) shows such a cage, optimized to operate at 440 and 600 nm. Here we notice that the metacages shown in Fig. 3(a) suppress the fields in a wide spectral range, so that

the average electric field inside the cage stays below 0.1 of the incident wave amplitude.

Table I summarizes the design parameters of the discussed metacages. Further studies show that the design of metacages with an acceptable performance is also possible with two-layer or even solid nanowires [29]. The benefit of three-layer structures discussed in this Letter is their high degree of varying parameters, either for specific wavelengths or for optimization of other performance parameters, such as the gap size.

In addition to shielding functionality, metacages can also be designed to show other interesting properties, e.g., arbitrary shapes, independence of the angle of incidence, physical connection between the two sides, and flexibility of selecting the central operating frequency. The last row of Table I corresponds to a metacage designed with suppressed backward scattering. Figure 4 demonstrates the shielding functionality and far-field scattering pattern. Such suppressed backward and enhanced forward scattering is very useful for many applications.

In conclusion, we have introduced a novel approach for designing optical shielding structures based on arrays of nanowires. We have designed, analyzed, and optimized metacages for both TE and TM polarizations with both hybrid and nonmetallic configurations, also confirming our results by numerical simulations based on a finite-element method. We have demonstrated that the introduced meta-shielding structures can maintain their functionality for an arbitrary shape due to the suppression of transmission by overlapping the energy flow separatrices. We have discussed a design of metacages for any selected wavelength in a wide spectral range, and have analyzed an interplay between gap size and efficiency of the field suppression.
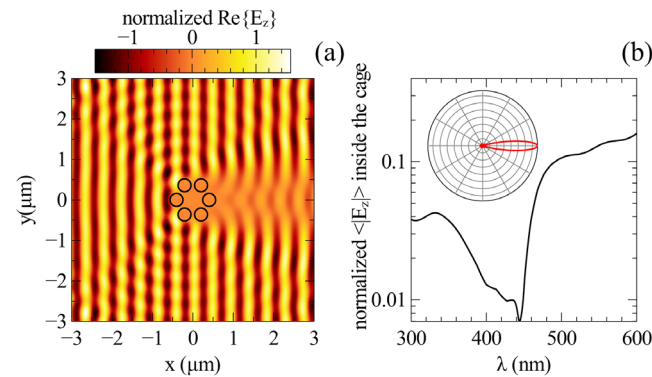
FIG. 4 (color online). (a) Real part of the field shows the absence of the backward reflection (the incident plane wave is propagating in the x direction). (b) Metacage keeps the shielding functionality. The inset shows the far-field scattering pattern; the metacage is made of gallium arsenide and titanium nitride [44] and the design parameters are listed in the last row of Table I.

*Corresponding author.
ali.mirzaei@anu.edu.au

[1] B. J. Eggleton, T. D. Vo, R. Pant, J. Schroder, M. D. Pelusi, D. Y. Choi, S. J. Madden, and B. L. Davies, Laser Photonics Rev. **6**, 97 (2012).

[2] A. Biberman and K. Bergman, Rep. Prog. Phys. **75**, 046402 (2012).

[3] S. Wu, S. Buckley, J. R. Schaibley, L. Feng, J. Yan, D. G. Mandrus, F. Hatami, W. Yao, J. Vukovi, A. Majumdar, and X. Xu, Nature (London) **520**, 69 (2015).

[4] L. Novotny and N. v. Hulst, Nat. Photonics **5**, 83 (2011).

[5] G. Wu, A. Mikhailovsky, H. A. Khant, C. Fu, W. Chiu, and J. A. Zasadzinski, J. Am. Chem. Soc. **130**, 8175 (2008).

[6] D. P. Morales, G. B. Braun, A. Pallaoro, R. Chen, X. Huang, J. A. Zasadzinski, and N. O. Reich, Mol. Pharmaceutics **12**, 600 (2015).

[7] H. Qiu, B. Cui, G. Li, J. Yang, H. Peng, Y. Wang, N. Li, R. Gao, Z. Chang, and Y. Wang, J. Phys. Chem. **118**, 14929 (2014).

[8] M. S. Yavuz, Y. Cheng, J. Chen, C. M. Cobley, Q. Zhang, M. Rycenga, J. Xie, C. Kim, K. H. Song, A. G. Schwartz, L. V. Wang, and Y. Xia, Nat. Mater. **8**, 935 (2009).

[9] L. Au, Q. Zhang, C. M. Cobley, M. Gidding, A. G. Schwartz, J. Chen, and Y. Xia, ACS Nano **4**, 35 (2010).

[10] J. Yang, D. Shen, L. Zhou, W. Li, X. Li, C. Yao, R. Wang, A. Mohamed El-Toni, F. Zhang, and D. Zhao, Chem. Mater. **25**, 3030 (2013).

[11] B. Therrien, ChemPhysChem **19**, 8378 (2013).

[12] R. M. Gorgoll, T. Tsubota, K. Harano, and E. Nakamura, J. Am. Chem. Soc. **137**, 7568 (2015).

[13] S. Feng and K. Halterman, Phys. Rev. Lett. **100**, 063901 (2008).

[14] V. C. Nguyen and L. Chen and K. Halterman, Phys. Rev. Lett. **105**, 233908 (2010).

[15] H. Yan, X. Li, B. Chandra, G. Tulevski, Y. Wu, M. Freitag, W. Zhu, P. Avouris, and F. Xia, Nat. Nanotechnol. **7**, 330 (2012).

[16] N. Engheta, Science **317**, 1698 (2007).

[17] K. Aydin, V. E. Ferry, R. M. Briggs, and H. A. Atwater, Nat. Commun. **2**, 517 (2011).

[18] S. Mann and E. Garnett, Nano Lett. **13**, 3173 (2013).

[19] J. Kupec, R. L. Stoop, and B. Witzigmann, Opt. Express **18**, 27589 (2010).

[20] C. Hagglund and S. P. Apell, Opt. Express **18**, A343 (2010).

[21] J. Motohisa and K. Hiruma, Jpn. J. Appl. Phys. **51**, 11PE07 (2012).

[22] Y. He, H. Deng, X. Jiao, S. He, J. Gao, and X. Yang, Opt. Lett. **38**, 1179 (2013).

[23] S. C. Chiu, H. C. Yu, and Y. Y. Li, J. Phys. Chem. C **114**, 1947 (2010).

[24] T. V. Teperik, F. J. Garcia de Abajo, A. G. Borisov, M. Abdelsalam, P. N. Bartlett, Y. Sugawara, and J. J. Baumberg, Nat. Photonics **2**, 299 (2008).

[25] Y. Radi, C. R. Simovski, and S. A. Tretyakov, Phys. Rev. Applied **3**, 037001 (2015).

[26] M. Kang, F. Liu, T. F. Li, Q. H. Guo, J. Li, and J. Chen, Opt. Lett. **38**, 3086 (2013).

[27] Y. Radi, V. S. Asadchy, S. U. Kosulnikov, M. M. Omelyanovich, D. Morits, A. V. Osipov, C. R. Simovski, and S. A. Tretyakov, ACS Photonics **2**, 653 (2015).

[28] C. A. Valagiannopoulos and S. A. Tretyakov, IEEE Trans. Antennas Propag. **62**, 5089 (2014).

[29] See Supplemental Material at http://link.aps.org/supplemental/10.1103/PhysRevLett.115.215501 for more information about the role of different materials, polarizations, and size values variation in metacages and their being independent from incident wave angle.

[30] C. A. Balanis, *Advanced Engineering Electromagnetics* (Wiley, New York, 1989).

[31] L. Schachter, *Beam-Wave Interaction in Periodic and Quasi-Periodic Structures* (Springer, New York, 2011).

[32] A. Mirzaei, A. Miroshnichenko, N. Zharova, and I. Shadrivov, J. Opt. Soc. Am. B **31**, 1595 (2014).

[33] U. Kreibig, J. Phys. F **4**, 999 (1974).

[34] A. Mirzaei, I. Shadrivov, A. Miroshnichenko, and Y. Kivshar, Opt. Express **21**, 10454 (2013).

[35] G. N. Watson, *A Treatise on the Theory of Bessel Functions* (University Press, Cambridge, 1966).

[36] G. O. Olaofe, Radio Sci. **5**, 1351 (1970).

[37] T. Tsuei and P. W. Barber, Appl. Opt. **27**, 3375 (1988).

[38] M. Quinten, *Optical Properties of Nanoparticle Systems: Mie and Beyond* (John Wiley & Sons, New York, 2010).

[39] A. Mirzaei and A. Miroshnichenko, Nanoscale **7**, 5963 (2015).

[40] D. E. Aspnes and A. A. Studna, Phys. Rev. B **27**, 985 (1983).

[41] E. Palik, *Handbook of Optical Constants of Solids* (Academic Press, New York, 1997).

[42] B. Lukyanchuk and V. Ternovsky, Phys. Rev. B **73**, 235432 (2006).

[43] B. Lukyanchuk, A. Miroshnichenko, and Y. Kivshar, J. Opt. Soc. Am. **15**, 073001 (2013).

[44] J. Pfluger, J. Fink, W. Weber, K. P. Bohnen, and G. Crecelius, Phys. Rev. B **30**, 1155 (1984).